# Very-long-chain fatty acids are required for cell plate formation during cytokinesis in Arabidopsis thaliana

Liên Bach, Lionel Gissot, Jessica Marion, Frédérique Tellier, Patrick Moreau, Béatrice Satiat-Jeunemaître, Jean-Christophe Palauqui, Johnathan A. Napier, Jean-Denis Faure

# Very-long-chain fatty acids are required for cell plate formation during cytokinesis in *Arabidopsis thaliana*

**Liên Bach[1], Lionel Gissot[1], Jessica Marion[2], Frédérique Tellier[1], Patrick Moreau[3], Béatrice Satiat-Jeunemaître[2], Jean-Christophe Palauqui[1], Johnathan A. Napier[4] and Jean-Denis Faure[1,*]**

[1]Institut Jean-Pierre Bourgin (IJPB), UMR1318 INRA-AgroParisTech, Saclay Plant Science (SPS), INRA Centre de Versailles-Grignon, Route de St-Cyr, 78000 Versailles, France
[2]Laboratoire Dynamique de la Compartimentation Cellulaire, CNRS, Institut des Sciences du Végétal, Centre de recherche de Gif (FRC3115), 91198, Gif-sur-Yvette Cedex, France
[3]Laboratoire Biogenèse membranaire, UMR5200 CNRS-Université Bordeaux 2, BP 33076 Bordeaux Cedex, France
[4]Department of Biological Chemistry, Rothamsted Research, Harpenden, Hertfordshire AL5 2JQ, UK
*Author for correspondence (faure@versailles.inra.fr)

## Summary

Acyl chain length is thought to be crucial for biophysical properties of the membrane, in particular during cell division, when active vesicular fusion is necessary. In higher plants, the process of cytokinesis is unique, because the separation of the two daughter cells is carried out by de novo vesicular fusion to generate a laterally expanding cell plate. In *Arabidopsis thaliana*, very-long-chain fatty acid (VLCFA) depletion caused by a mutation in the microsomal elongase gene *PASTICCINO2* (*PAS2*) or by application of the selective elongase inhibitor flufenacet altered cytokinesis. Cell plate expansion was delayed and the formation of the endomembrane tubular network altered. These defects were associated with specific aggregation of the cell plate markers YFP–Rab-A2a and KNOLLE during cytokinesis. Changes in levels of VLCFA also resulted in modification of endocytosis and sensitivity to brefeldin A. Finally, the cytokinesis impairment in *pas2* cells was associated with reduced levels of very long fatty acyl chains in phospholipids. Together, our findings demonstrate that VLCFA-containing lipids are essential for endomembrane dynamics during cytokinesis.

**Key words:** Phospholipids, Cell plate, Vesicle trafficking, Endocytosis, Root development

## Introduction

Very-long-chain fatty acids (VLCFAs) are acyl chains greater than 18 carbons in length, and are now known to be membrane components in all eukaryotic cells (Bach and Faure, 2010; Schneiter et al., 2004; Schneiter et al., 1996). VLCFAs are synthesised by the elongation of C16 and C18 precursor fatty acids by the sequential addition of C2 moieties from malonyl-CoA, a reaction catalysed by the ER membrane-bound microsomal elongase complex. This elongase complex carries out four distinct and sequential enzymatic reactions. Chain elongation is initiated by the condensation of the C16/18-CoA with malonyl-CoA to form 3-keto-acyl-CoA. In animals and yeasts, this reaction is carried out by the keto-acyl-CoA synthase (KCS or condensing enzymes), which is encoded by the multigenic *ELO* gene family (Paul et al., 2006). In plants, the KCS activity is encoded by two structurally unrelated gene families: in *Arabidopsis* there is a large family of *FAE1*-like genes as well four members of the unrelated *ELO*-like class of condensing enzymes (Dunn et al., 2004). Both forms of KCS generate 3-keto-acyl-CoA, which is then reduced by the keto-acyl-CoA reductase (KCR) to form 3-hydroxy-acyl-CoA, which is in turn dehydrated by the 3-hydroxy-acyl-CoA dehydratase (PAS2) into an enoyl-CoA (Bach et al., 2008). Finally, this enoyl-CoA is reduced by the enoyl-CoA reductase (ECR) to generate an acyl chain extended by two carbons (Nugteren, 1965).

Depending on their chain length and their level of unsaturation, VLCFAs show a wide range of physiological and structural functions, making them crucial for many biological processes such as cell expansion, cell proliferation or differentiation (Bach and Faure, 2010).

VLCFAs are commonly found in neutral lipids such as triacylglycerols (TAGs) or storage lipids in adipose tissue or seeds, but in animals they also have a structural role in skin-barrier function as protective lipids (Westerberg et al., 2004) or epicuticular waxes and suberin, which prevent desiccation and physical damage in plants. Furthermore, VLCFAs are also found in phospholipids and sphingolipids, where they probably determine the properties of cell membranes. Different subcellular membranes have a discrete lipid composition, and even within the same membrane the lipid distribution differs between the two sides of the lipid bilayer and displays different degrees of lateral organization (Lingwood and Simons, 2010; van Meer, 1989). Fatty acyl chain length was also found to be crucial for membrane curvature. In yeast, the isolation of a conditional acyl-CoA carboxylase mutant demonstrated that a reduced amount of 26:0-containing lipids was linked to defects in nuclear pore formation. In particular, C26-phosphatidylinositol was found to be essential for stabilizing highly curved membrane structures (Schneiter et al., 2004). Sphingolipids, sterols and saturated phospholipids also demonstrate domain-forming properties that allow them to trigger the formation of microdomains (so-called ‘lipid rafts’) involved in the sorting of certain plasma membrane proteins, cell stability at the cell surface and endocytosis (Borner et al., 2005; Ikonen, 2001;

Mongrand et al., 2004; Wang and Chang, 2002). VLCFAs were recently shown to be necessary for coordinating plasma membrane deformation and forming specialized membrane domains required for actin ring constriction and stability at the cortex (Szafer-Glusman et al., 2008). Interestingly, a loss-of-function mutation in BOND, a *Drosophila* member of the Elovl KCS family led to cytokinesis defects in spermatocytes. In particular, defects in the synthesis of VLCFAs affected the contraction of the actin ring, as well as the stabilization of the midzone microtubules, resulting in a dramatic block of cleavage furrow ingression in early telophase (Szafer-Glusman et al., 2008).

Importantly, cytokinesis in vascular plants is strikingly different to that in other higher eukaryotes because the separation of the two daughter cells requires a new structure (called the cell plate), the formation of which requires the supply of new material to form plasma membrane and cell wall. In *Arabidopsis* roots, cell plate formation can be completed in less than 30 minutes and requires the creation of one-third of the original cell surface area (Jürgens and Pacher, 2004). In these conditions, rapid delivery of new material to a precise subcellular location implies specific targeting and rapid vesicular trafficking. Plant cells control cytokinesis by building the phragmoplast, which includes microtubules and actin-based structures that allow unidirectional vesicle delivery and fusion, generating the cell plate. Most of these vesicles are derived from the endoplasmic reticulum (ER) and Golgi complex (Alberts et al., 2002; Reichardt et al., 2007), but endocytosis was also suggested to contribute significantly to the accumulation of plasma membrane proteins in the nascent cell plate (Dhonukshe et al., 2006). Recently, sterol-dependent endocytosis was found to restrict lateral diffusion of the cytokinesis-specific syntaxin KNOLLE and to maintain its correct localization at the plane of division (Boutte et al., 2009).

Although it is agreed that vesicle fusions leading to the tubulovesicular and tubular networks necessary for plant cell plate formation and growth require SNARE proteins and small Rab GTPase (for reviews, see Lipka et al., 2007; Molendijk et al., 2004), the role of endomembrane lipids remains unclear. Previously, PAS2 protein was characterized as the 3-acyl-CoA dehydratase involved in the elongation of the VLCFAs. The absence of PAS2 led to a reduction of VLCFAs in three major lipid classes (triacylglycerol, epicuticular waxes, sphingolipids) resulting in profound developmental defects throughout the plant (Bach et al., 2008). Interestingly, the *pas2* mutant displayed abnormal cell division patterns and ectopic expression of cell cycle markers, suggesting that PAS2 activity is involved in cell division (Bellec et al., 2002). However, the precise role of VLCFAs and VLCFA-containing lipids during cell division remained to be determined.

Here, we demonstrate that the *pas2* mutant displays reduced root growth that was caused by a delay in cell plate establishment during cytokinesis. Live-cell imaging associated with ultrastructure analysis confirmed that the cell plate structure was altered and that endomembrane dynamics was modified. These defects were correlated with the reduction of very long fatty acyl chains into phosphatidylethanolamine and phosphatidylserine phospholipid pools, suggesting that the acyl chain length in endomembranes are crucial for cell plate formation and cytokinesis.

## Results

### Reduced *pas2* root growth is associated with higher incidence of mitotic cells

The *pas2*-1 mutant was initially characterized by ectopic cell proliferation and competence for differentiated tissue to divide in the shoot (Bellec et al., 2002; Faure et al., 1998), but also by its shorter primary root (supplementary material Fig. S1A). The role of PAS2 during root development was first investigated by analysing its expression of the p*PAS2:PAS2-GFP* construct. This construct was fully functional because it complemented all *pas2-1* developmental defects (supplementary material Fig. S2A). Stable expression of p*PAS2:PAS2-GFP* in several independent transgenic lines showed that *PAS2* was expressed in the root tip (supplementary material Fig. S2B). Primary root length of 5-day-old *pas-2-1* root was 50% of that in the wild type (supplementary material Fig. S1A), which could result from altered cell division or elongation. Root growth has the advantage of spatially uncoupling cell division, elongation and differentiation, with a division zone at the tip, followed by an elongation zone that precedes the differentiated part consisting of the rest of the root. We therefore measured the total length and the number of cells of the cell division zone. *pas2-1* roots exhibited shorter division zone (supplementary material Fig. S1B), but the cortical cell number was similar to that in the wild type ($29.25 \pm 2.11$ and $31.43 \pm 2.20$, respectively) (supplementary material Fig. S1C), suggesting a slight reduction in cell size in the mutant. A similar effect could also be seen in the elongation zone, which was slightly shorter in the *pas2-1* mutant compared with the wild type (supplementary material Fig. S2C). Nevertheless, the reduction in the cell division and elongation zones could not fully account for the reduced root growth. Alternatively, reduced root growth could be caused by a delay in cell division. To investigate cell division frequency, we monitored the expression of the mitotic cyclin CYCB1 (*pCYCB1:db-GUS*) in *pas2-1* primary root tip. The number of GUS-positive (as an indicator of mitosis) cells was higher in the *pas2-1* mutant ($13.64 \pm 3.20$) than in the wild type ($8.63 \pm 2.25$), showing that although root growth is delayed in the mutant, the *pas2-1* root has a higher number of dividing cells (supplementary material Fig. S1D).

### *Pas2-1* mutation enhances the number of cells in late mitosis

Because the *pas2-1* mutation did not cause an increase in the number of cells in the division zone, the apparent enhanced mitotic activity might result from an early entry into mitosis or extended mitotic phases. We investigated whether the relative distribution of mitotic stages was modified by the *pas2-1* mutation. To determine precisely the different phases of mitosis, phragmoplast, cell plate and nuclear DNA were observed in fixed *pas2-1* and wild-type roots. The microtubule network was labelled with anti-tubulin antibodies and the cell plate was defined with antibodies against the syntaxin KNOLLE, which specifically labels the cell plate during cytokinesis (Lauber et al., 1997). Chromatin and condensed chromosomes were counterstained with DAPI. In prophase, metaphase or anaphase, the KNOLLE protein was associated with dispersed punctuate structures inside cells (supplementary material Fig. S3A–C). Then, from the early telophase to the end of cytokinesis, KNOLLE was accumulated in the mid plane of the cell to form the cell plate in association with the expanding annular phragmoplast microtubules (supplementary material Fig. S3D–

F). In the *pas2-1* mutant, microtubules organized in the mitotic spindle and phragmoplast in a very similar pattern to that in the wild type (supplementary material Fig. S3G,H).

The different stages of mitosis were quantified (with the caveat that it was sometimes difficult to discriminate between the late stages, i.e. early telophase, telophase and cytokinesis, in the *pas2-1* mutant because the KNOLLE-labelled cell plate was often observed in cells at an undefined mitotic stage, see below). To get a quantitative estimate, all the mitotic stages showing a clear KNOLLE-labelled cell plate were combined into one experimental group spanning the early telophase, telophase or cytokinesis stages (Fig. 1). The relative number of cells at the early stages of mitotis (prophase, metaphase and anaphase) was slightly lower in the *pas2-1* mutant compared with the wild type. By contrast, *pas2-1* roots showed a high proportion of cells in the late mitotic stages (6.74%) compared with the wild type (4.42%), suggesting that the lack of VLCFAs impaired cell plate progression.

### Cell plate formation is delayed in the *pas2-1* mutant

The enhanced incidence of *pas2-1* cells in late mitosis could result from delayed establishment of the new cell plate. To investigate the kinetics of cell plate formation, we used the fluorescent lipophilic styryl dye FM4-64, which is rapidly targeted to the emerging cell plate in early telophase (Dettmer et al., 2006).

Real-time kinetics analysis of cell plate formation was carried out by imaging pRabA2a:YFP-RabA2a-expressing roots stained with FM4-64. RabA2a was previously described as a small GTPase that labels both early endosomes in interphasic cells and the cell plate during cytokinesis (Chow et al., 2008). The first steps of cell plate formation consist of very rapid aggregation of RabA2a vesicles into a plate structure, and no difference could be distinguished between wild-type cells and the *pas2-1* mutant (Fig. 2A). Once the cell plate is formed, it extends until it reaches the lateral membranes (Fig. 2B). Cell plate expansion kinetics showed that the cell plate required more time to complete in the *pas2-1* mutant compared with the wild type (Fig. 2B,C). Cell plate kinetics was measured based on the ratio of cell plate length per cell width of dividing root tip cells (Fig. 2C). In the wild type, the cell plate was nearly completed in 30–40 minutes, whereas the *pas2-1* cell plate required more than 120 minutes to establish (Fig. 2B,C). In contrast to the wild-type cell plate, which grew constantly with a velocity of 13 nm/minute, the *pas2-1* cell plate completion showed two distinct growth phases: for at least 50 minutes, cell plate extension did not progress significantly, it then resumed growth and gradually completed cytokinesis at a velocity of 5 nm/minute (50% of the wild-type value).

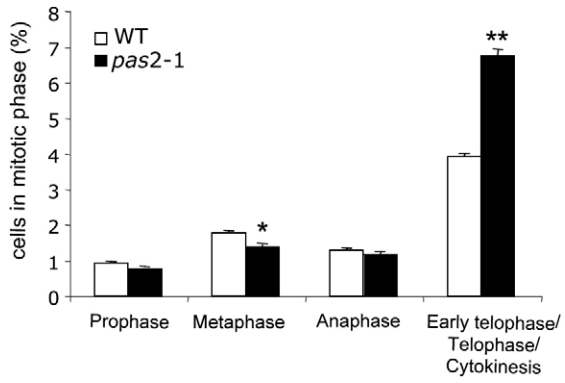


**Fig. 1. The *pas2-1* mutant shows an increase in cell-plate-forming cells.** Relative number of cells in the different mitotic stages in *pas2-1* and wild-type root tips. Mitotic stages were determined by DAPI staining and immunolocalization as described in supplementary material Fig. S1. Data are the means (±s.d.) of two replicates of ten independent root tips gathering at least 500 cells per root. Significant differences with Student's *t*-test are indicated (**P*≤0.05; ***P*≤0.01).

### Defective cell plate formation in the *pas2-1* mutant involves specific aggregation of YFP–RabA2a and KNOLLE

In about 20% of cases, cell plate extension in *pas2-1* was eventually stopped before completion, regressing to form heterogeneous aggregates labelled by both YFP–RabA2a and FM4-64 (Fig. 3A,B and supplementary material Fig. S4A–C). In addition, 13% of *pas2-1* root cells showed aggregation of YFP–RabA2a, which corresponds to the mitotic index in the mutant (supplementary material Fig. S1D). Aggregates were occasionally directly associated with the extremity of the cell plate, suggesting that they were formed at the point of vesicular fusion (Fig. 3C). This cytokinetic defect in *pas2-1* cells was not associated with the aggregation of the prevacuolar marker GFP–RabF2b, suggesting some specificity to early endosome compartments (supplementary material Fig. S5A). We also occasionally observed fragmented cell plates in *pas2-1* cells, which eventually regressed, leaving cell wall stubs at the junction sites with the plasma membrane (supplementary material Fig. S4D). Usually, these cell wall stubs were correlated with binucleate or multinucleate cells caused by successive rounds of mitosis and nuclear division without completed cytokinesis. Binucleated cells were never observed in the *pas2-1* mutant, probably because VLCFA depletion was not sufficient for complete cell plate arrest. Indeed, *pas2-1* cell plate formation could resume and eventually progress to completion (supplementary material Fig. S4E). This observation would also explain the low number of cells with defective cell plates. Indeed, only 4.5% of *pas2-1* mitotic cells showed abnormal cell plates. However, inhibition of elongase activity with the ketoacylsynthase inhibitor flufenacet led to a cytokinetic defect and binucleated cells (supplementary material Fig. S5B,C). Flufenacet was previously shown to specifically inhibit several KCS and to lead to post-genital organ fusion, a hallmark of elongase mutants (Trenkamp et al., 2004). Flufenacet treatment of *Arabidopsis* seedlings showed that VLCFA elongation was indeed inhibited, with a reduction in C22, C24 and C26 fatty acids (supplementary material Fig. S6). Interestingly, C20:1 and C20:2 levels were increased, suggesting that flufenacet is targetting KCS involved in C20+ elongation. As for *pas2-1,* flufenacet induced YFP–RabA2a aggregation, but also ectopic accumulation in mature membrane (supplementary material Fig. S5C,D). In the conditions of YFP–RabA2a aggregation, no effect of flufenacet was observed on GFP–RabF2b, SNX1–GFP and VHA1a–GFP markers, indicating that prevacuolar and late endosomes compartments, as well as TGN, were not globally modified by VLCFA depletion (supplementary material Fig. S5E).

VLCFA depletion induced by *pas2-1* mutant or by flufenacet appeared to perturb preferentially YFP-RabA2a compartments during cytokinesis but also in interphasic cells (Fig. 3C, top and

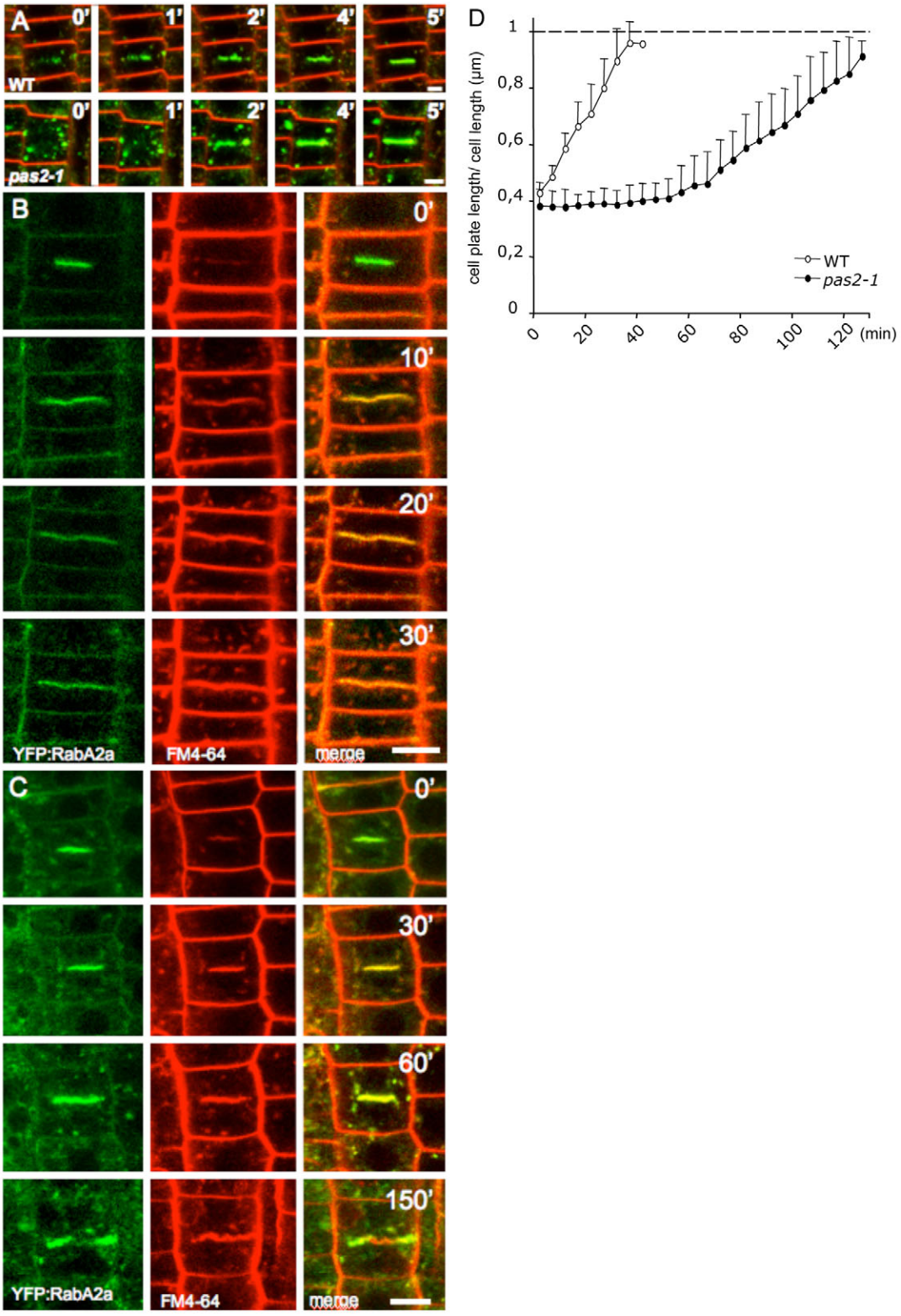


**Fig. 2. Cell plate formation is delayed in *pas2-1* mutant.** (**A**) Kinetics of early phases of cell plate formation in epidermal cells of 5-day-old root tips from wild-type (top) and *pas2-1* mutant (bottom) expressing *pRab-A2a:YFP-RabA2a* (green) and stained with FM4-64 (red). Scale bar: 5 µm. (**B**,**C**) Kinetics of cell plate formation in epidermal cells of 5-day-old root tips from wild-type (A) and *pas2-1* mutant (B) expressing *pRab-A2a:YFP-Rab-A2a* (green) and stained with FM4-64 (red). Scale bar: 5 µm. Time is shown in top right corner of all images in minutes. (**D**) Cell plate relative size (means + s.d.) determined by the ratio cell plate length per cell width in wild-type and *pas2-1* seedlings shown in A,B ($n$=10).

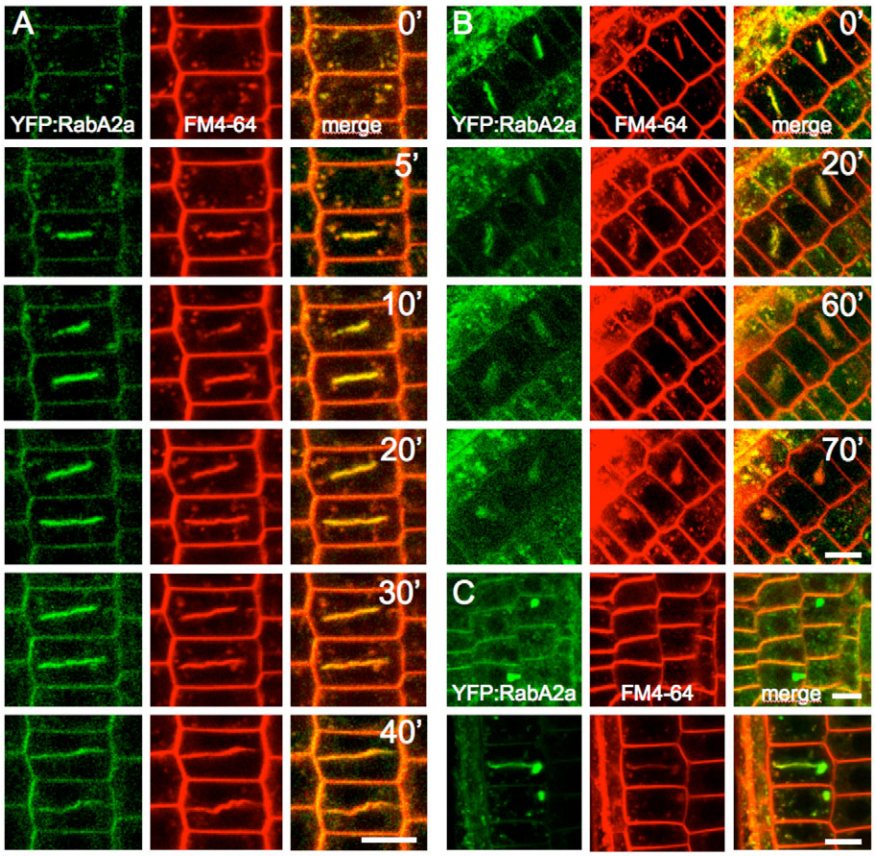


**Fig. 3. Arrested *pas2-1* cell plates break up in aggregated material.** (**A**) Cell plate formation in wild-type epidermal cells expressing *pRab-A2a:YFP-RabA2a* (green) incubated with FM4-64 (red). Scale bar: 5 µm. (**B**) Arrested cell plates in *pas2-1* mutant regress and aggregate into YFP–RabA2a (green)- and FM4-64 (red)-labelled compartments. (**C**) YFP-RabA2a aggregates (green) are present in interphasic (top) and dividing cells (bottom) where they colocalize with FM4-64 (red) close to the cell plate. Scale bars: 5 µm.

Fig. 4C). To test whether these aggregates labelled by YFP–RabA2a and observed in both dividing and interphasic cells were related to cell plates in regression, we also monitored the distribution of KNOLLE. YFP–RabA2a aggregates were always labelled by KNOLLE during metaphase and anaphase–telophase when the cell plate is normally emerging (Fig. 4A,B). Interestingly, the aggregates labelled with YFP–RabA2a and KNOLLE were either associated with the expanding cell plate or scattered along a pseudo-cell-plate line, suggesting that these aggregates are directly related to the formation of the cell plate (Fig. 4A,B). In contrast to dividing cells, no KNOLLE aggregates could be observed in interphasic cells, suggesting that KNOLLE could still undergo post-mitotic turnover even in aggregates (Fig. 4C). Nonetheless, KNOLLE-labelled ectopic cell plates could occasionally be found in interphasic *pas2-1* cells, indicating that misorganized cell plate structure could remain after cell division is completed (Fig. 4D). Interestingly, similar cytokinetic defects with ectopic KNOLLE-labelled cell plate could be observed in the other VLCFA-defective *pasticcino* mutant *pas3-1* (supplementary material Fig. S3I).

### The cell plate ultrastructure is modified in *pas2-1* cells

To gain insights into the cause of cell plate delay or fragmentation, transmission electron microscopy imaging was carried out on *pas2-1* and wild-type root tips. Electron micrographs of *pas2-1* dividing cells clearly show that the mutation interferes with several aspects of membrane fusion of cell plate material. In the early stage of cell division, both wild-type and *pas2-1* cells showed an accumulation of vesicle fusion in the equatorial plane, forming an electron-dense tubulovesicular network typical of the early events of cell plate formation (data not shown) (Samuels et al., 1995). However, in the subsequent stages, *pas2-1* cell plate development showed significant modifications compared with that in the wild type. In control cells, the cell plate changed from a tubulovesicular network into a more open, smooth and straight tubular network (Fig. 5A). At the same time, the lumen of the network became less electron dense, probably because of the accumulation of new cell wall components (callose, cellulose). By contrast, in *pas2-1* cells at late telophase, a large gap of cytoplasm between the tubular elements was often observed, even at a stage where both nuclei were recondensed. The conversion of the cell plate from the tubulo-vesicular network into this typical tubular network was also modified (Fig. 5B). The tubular network was thinner than in control cells, exhibited a 'wavy' profile, and maintained electron-dense characteristics from the first stage of tubulovesicular network formation. Despite these defects, the *pas2-1* cell plate was able to resume growth and reached completion, with electron-dense material that eventually disappeared, similarly to that in control cells. However, the *pas2-1* mature cell plate still exhibited this wavy profile (characteristic of an early stage), whereas control cell plates showed a straight structure (Fig. 5C,D). Even after completion, cell plate material still anchored at the plasma membrane was observed, probably as a result of an abortive cell plate (Fig. 5E). The presence of numerous autophagosomal structures in these cells suggests that there is intense membrane-recycling activity to dispose of the ectopic membrane (Fig. 5E). Another unusual feature was the

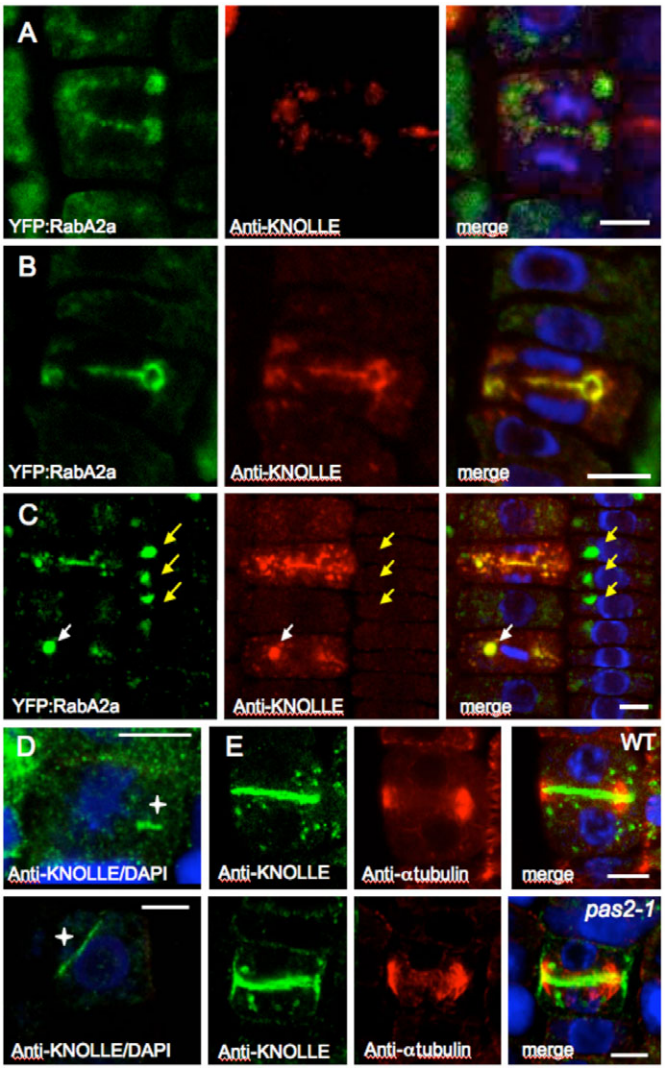


**Fig. 4. Aberrant *pas2-1* cytokinesis is associated with ectopic accumulation of cell plate markers.** (**A**,**B**) Immunolocalization of KNOLLE (red) in telophase cells of *pas2-1* root tip expressing YFP–RabA2a (green) show fragmented cell plate surrounding condensed chromosomes (A) or loop-like structures at the end of the cell plate (B). Condensed chromosomes are visualized by DAPI staining (blue). Scale bars: 5 µm. (**C**) YFP–RabA2a aggregates (green) colocalize with endogenous KNOLLE (red) during cell division (white arrow) but are distinct in interphase cells (yellow arrows). Scale bar: 5 µm. (**D**) KNOLLE-labelled ectopic cell plates (cross) are observed in *pas2-1* interphase cells. Scale bar: 5 µm. (**E**) Enlarged KNOLLE-labelled cell plate is associated with mislocalization of KNOLLE protein to the lateral sides of cells in *pas2-1* mutant cells (bottom) in contrast to the wild type, where KNOLLE is restricted to the cell plate (top). Scale bars: 5 µm.

presence of electron-dense vesicular and tubular structures within the cytoplasm (Fig. 5F, arrows). They were often observed in cells having already completed their cytokinetic process and were reminiscent of the tubulovesicular structures that usually form at the initial stage of cell plate development.

### Role of endocytic and secretory pathway in *pas2-1* defective cytokinesis

The delay in cell plate formation, as well as the aggregation of the cell plate markers, could indicate that vesicular trafficking to the new membrane is modified by the depletion of VLCFAs associated with the *pas2-1* mutation. Cell plate formation requires not only the secretory pathway to transport the different cargoes to the newly formed membrane, but also endocytosis to recycle plasma membrane components (Dhonukshe et al., 2006; Reichardt et al., 2007). The involvement of endocytosis in the *pas2-1* cytokinesis defect was suggested by the fact that at the end of mitosis, KNOLLE was often found mislocalized in lateral membranes of the dividing cell (Fig. 4E). Similar labelling could also be observed in the other *pasticcino* mutants (supplementary material Fig. S3J). Interestingly, this labelling of lateral membranes was reminiscent of what was previously observed in the endocytosis mutants *arf1* and *drp1A* or in tyrphostin-A23-treated wild-type cells (Boutte et al., 2006). Sterol depletion in the *cpi-1* mutant similarly to VLCFA depletion in *pas2-1* cells, also resulted in KNOLLE distribution in lateral membranes (Boutte et al., 2006). To confirm the effect of VLCFA depletion on endocytosis, FM4-64 pulse-chase experiments were carried out in *pas2-1* and wild-type root tips. FM4-64 is usually used as an endocytic marker because it internalizes and rapidly labels endosomal compartments and the cell plate (Geldner et al., 2003). After a short labelling, FM4-64 was washed away and its internalization was monitored to determine the endocytic time when clear FM4-64 labelling was visible inside a cortical cell (Fig. 6A). In contrast to the wild type, where the average endocytic time was 5 minutes, *pas2-1* cortical cells required about 20 minutes to internalize FM4-64, indicating that endocytosis was strongly delayed in the *pas2-1* mutant (Fig. 6B).

To investigate the involvement of endosomal trafficking in the *pas2-1* mutant, we used the anterograde transport inhibitor brefeldin A (BFA), which targets the ADP ribosylation factor and guanine nucleotide exchange factors (ARF-GEFs) leading to reversible inhibition of vesicle secretory trafficking (Geldner et al., 2003; Renault et al., 2002). BFA inhibits in particular endosomal recycling to the plasma membrane of several proteins such as PIN FORMED 1 (PIN1) (Steinmann et al., 1999). BFA application results in the accumulation of PIN1 in large endosomal and Golgi aggregates referred as BFA compartments (Boutte et al., 2006). The sensitivity of PIN1 distribution to different concentrations of BFA was investigated in wild-type and *pas2-1* primary roots. BFA was applied to wild-type and *pas2-1* seedlings for 30 minutes and the occurrence of PIN1–GFP in large BFA compartments was observed in the stele (Fig. 7A). At 50 µM BFA, both wild-type and *pas2-1* primary roots showed saturating formation of BFA compartments labelled with PIN1–GFP (Fig. 7B). However, at 25 µM BFA, less than 50% of *pas2-1* cells were BFA responsive compared with 75% in the wild type, indicating that PIN1 trafficking is less sensitive to BFA in the *pas2-1* background. Similar finding was also observed with YFP–RabA2a (Fig. 7C) indicating that both recycling membrane proteins, similarly to resident early endosomes were more resistant to BFA in the context of *pas2-1*. However, the Golgi marker QUASIMODO2 (QUA2–GFP), which does not cycle with the plasma membrane, showed similar BFA sensitivity in *pas2-1* and wild-type cells (Mouille et al., 2007). VLCFA depletion could modify BFA sensitivity by inhibiting endocytosis or by enhancing trafficking through early endosomal compartments. We investigated the latter effect in the *pas2-1* mutant by measuring YFP–RabA2a recovery at the cell plate after photobleaching (supplementary material Fig.

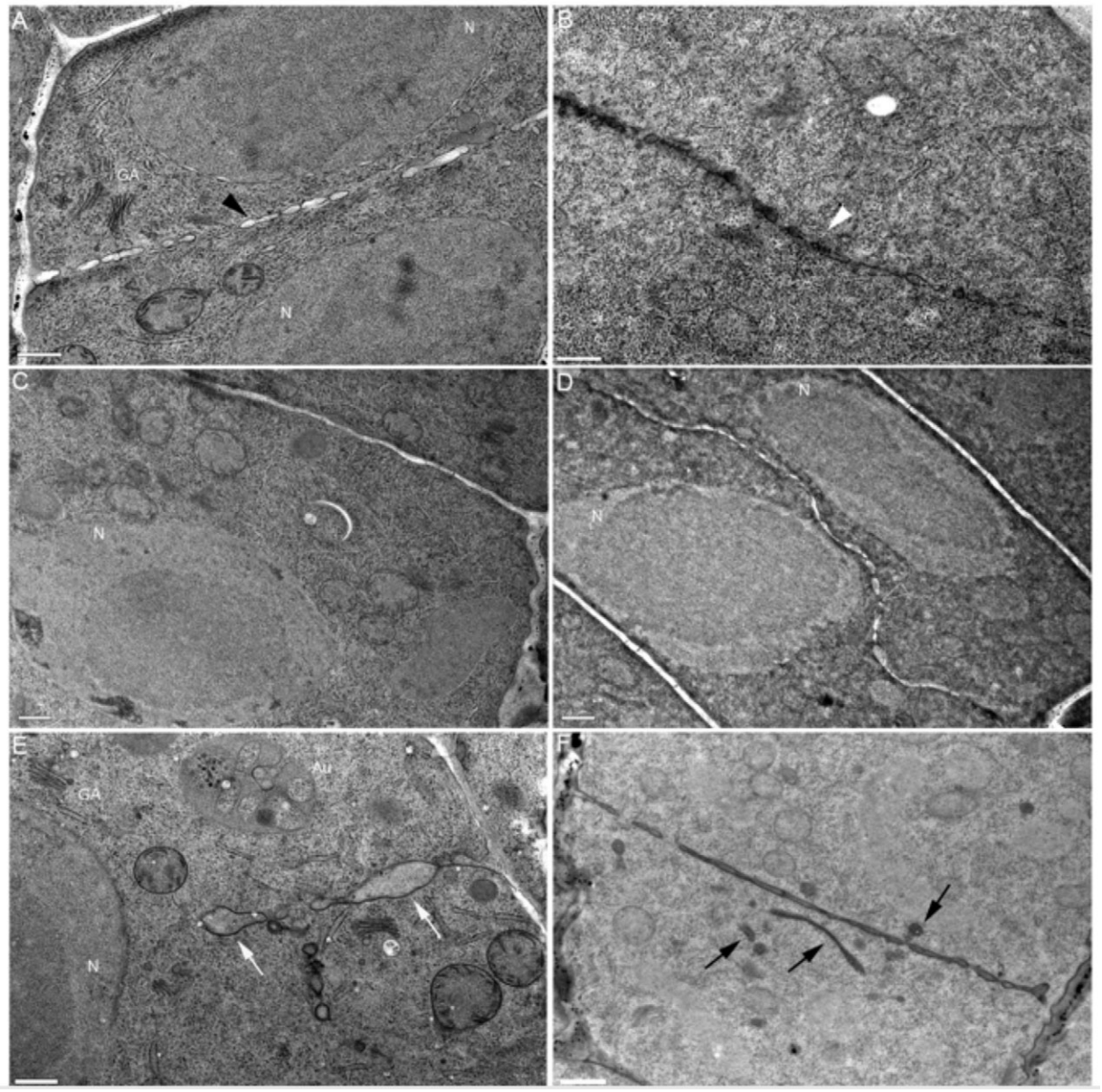


**Fig. 5. Cell plate ultrastructure is altered in *pas2-1* mutant.** (**A**) Wild-type telophase with a typical cell plate (arrowhead) between two nuclei (N). Note the straight 0.25-µm-thick cell plate with vesicular and tubular structures and no electron-dense content. (**B**) Structure of *pas2-1* telophase cell. Note the thinner tubular network with electron-dense lumen and wavy profile of the cell plate (white arrowhead) compared with A. (**C**) Completed wild-type cell plate in late-telophase–interphase. (**D**) Structure of *pas2-1* cell plate in late telophase. Note cell plate undulation between the two nuclei (N). (**E**,**F**) Abnormal *pas2-1* cell plate. Abortive cell plate (white arrows) is still attached to the mother cell wall (E). Note that *pas2-1* mutation does not modify Golgi ultrastructure (GA) but induce the presence of autophagic-like structure (Au). (F) Cell plate-like fragments in late-telophase–interphase *pas2-1* cells are usually filled with electron-dense materials (black arrows) (F). Scale bars: 500 nm.

S7A). The maximum recovery of YFP–RabA2a fluorescence at the cell plate was reached after about 3 minutes in both wild-type and *pas2-1* cells (supplementary material Fig. S7B). No obvious difference could be seen in the kinetic recovery, indicating that VLCFA depletion did not impair YFP–RabA2a trafficking from endosomal pools to the expanding cell plate. Similarly, treatment with flufenacet did not modify the apoplastic distribution of the secreted LeAGP1 marker (Estevez et al., 2006), confirming the minor contribution of VLCFA to the secretory pathway (supplementary material Fig. S7C).

### VLCFA phospholipids, but not sterols, are reduced in *pas2-1* mutant root

Finally, we investigated whether the different defects in cell plate formation and endomembrane dynamics were correlated with changes in membrane lipid composition. Biological bilayer membranes consist of polar lipids, predominantly glycerolipids associated with sterols and sphingolipids. Among the glycerolipids, the phospholipids are the most representative. It has been postulated that VLCFAs, through their involvement in structural membrane lipids, can influence membrane dynamics (membrane bending and

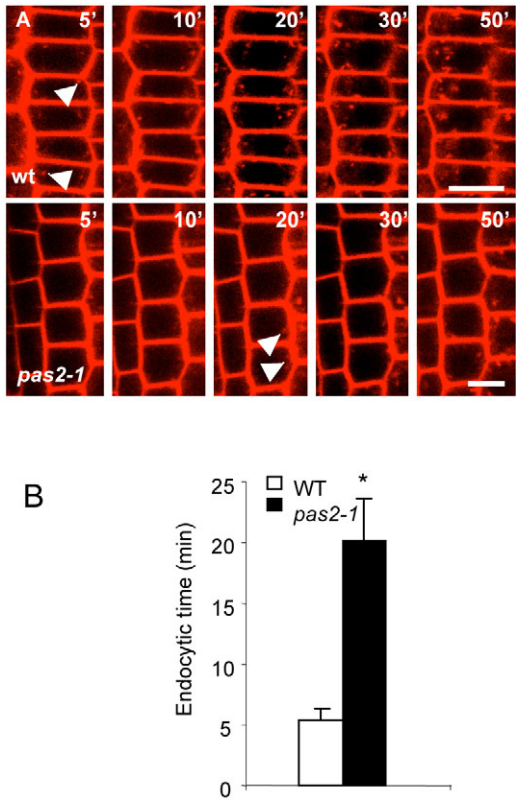


**Fig. 6. Endocytosis is delayed in *pas2-1* mutant.** (**A**) Kinetic of FM4-64 uptake (red) was monitored in wild-type (top) and *pas2-1* (bottom). Time is giving in minutes. Arrows indicate the first visible endosomes in the cortex cells. Scale bars: 5 µm. (**B**) FM4-64 uptake is delayed in *pas2-1* cortical cells. Average endocytic time was measured by determining for each cell, the time required for the internalization of FM4-64. Data are means + s.d. ($n$=20); *$P$<0.05.

fusion, membrane microdomains) (Schneiter et al., 2004). In a previous study, we reported that the levels of sphingolipids with very long acyl chains were strongly reduced in *pas2-1* seedlings compared with levels in the wild type (Bach et al., 2008). Here, we compared the levels of phospholipids in *pas2-1* and wild-type cells (Fig. 8, supplementary material Figs S8 and S9). Phosphatidylethanolamine (PE) and phosphatidylserine (PS) are the two phospholipids that contain significant amounts of VLCFAs, and are known to be fusogenic phospholipids (Mima and Wickner, 2009; Moreau et al., 1992). In roots, VLCFAs are almost exclusively present in PE. VLCFA-containing PE levels (PE≥C40) were almost absent in *pas2-1* mutant compared to the wild type and a similar effect could be observed in VLCFA-containing PS (supplementary material Fig. S8). The effects of *pas2-1* on VLCFA-containing-phospholipids was also confirmed in shoots where the levels of both VLCFA PE and VLCFA PS were strongly reduced by 80% and 60%, respectively (supplementary material Fig. S9). Interestingly, in both roots and shoots, the reduction in VLCFA phospholipids was correlated with enhanced levels of long acyl chain PE and PS. A similar compensatory effect was also found for sterols. Total sterols represented 12.9±0.4% of total lipids ($n$=3) in *pas2-1* seedlings compared with 8.8±0.3% ($n$=4) for the wild type, indicating that the reduction in VLCFAs is correlated with enhanced sterol levels.

## Discussion

Complete loss of PAS2 function leads to embryo lethality, demonstrating that very long acyl chains are essential for cell viability (Bach et al., 2008). However, weak alleles partially impairing *PAS2* function still significantly reduced accumulation of VLCFAs and caused strong developmental defects (Bach et al., 2008; Bellec et al., 2002). We found that the *pas2-1* reduction of VLCFAs levels led to specific accumulation of cells in late mitosis with delayed, unfinished or abnormal cell plates. When so delayed, cell plate expansion later resumed at a velocity lower than observed in the wild type. However, when cell plate expansion was arrested for more than 1 hour, it eventually regressed and collapsed, resulting in aggregation of specific cell plate proteins and endocytic markers. The direct involvement of VLCFAs in cell plate formation was confirmed by the presence of defective cytokinesis in the *pasticcino1* and *pasticcino3* mutants, both of which were recently characterized as VLCFA-defective mutants impaired in protein trafficking to the plasma membrane (Roudier et al., 2010). Moreover, cell plate defects and specific YFP–RabA2a aggregation was also confirmed in cells in which VLCFA synthesis was chemically inhibited.

Cell plate formation is a multistep process that starts during late anaphase and is completed by late telophase (Samuels et al., 1995; Van Damme et al., 2008). Reduction of VLCFA did not affect the targeting of vesicles to the equatorial plane or the first fusion events, which typically take place shortly after to generate the tubulo-vesicular network. However, several observations suggest that VLCFAs are essential later for cell plate expansion and the synthesis of a new plasma membrane and cell wall. First, *pas2-1* cell plates combined a tubulo-vesicular network typical of the initial stage and an open tubular network typical of the telophase stage, indicating a delay of vesicle fusion into tubules. Similar structures have already been described as a hallmark of the degradation of abnormal cell plates (Hepler and Bonsignore, 1990). Second, the presence of wavy profiles in almost completed cell plates that were not always positioned in the expected perpendicular plane is very unusual because such an undulating pattern is typical of early phases of cell plate assembly. Flattening and stiffening seem to occur when cellulose starts to be deposited during the late tubular network stage (Samuels et al., 1995). Finally, the occurrence of fragmented cell plates and related materials in association with autophagic structures indicates that cell plate formation was aborted and the remaining structures recycled. Once the cell plate is formed and anchored, the maturation phase takes place with additional fusion events to close the fenestrate but also requires endocytosis to redefine membrane polarity and to remove excess cellulose and callose (Samuels et al., 1995; Segui-Simarro et al., 2004). Callose was postulated to mechanically stabilize the membrane networks, eventually flattening the structure into a plate-like shape (Samuels et al., 1995). The essential role of callose during cytokinesis was recently demonstrated with the functional analysis of the callose synthase *GSL8* (Chen et al., 2009), where reduction of callose deposition at the cell plate associates with defective cell plate and the presence of cell wall stubs. Altogether, these results suggest that VLCFAs could be directly involved in the dynamics of cell plate expansion by providing the appropriate lipid environment for membrane fusion and recycling.

Mutation in *PAS2* led to the reduction of VLCFAs, which are themselves components of several classes of lipids including

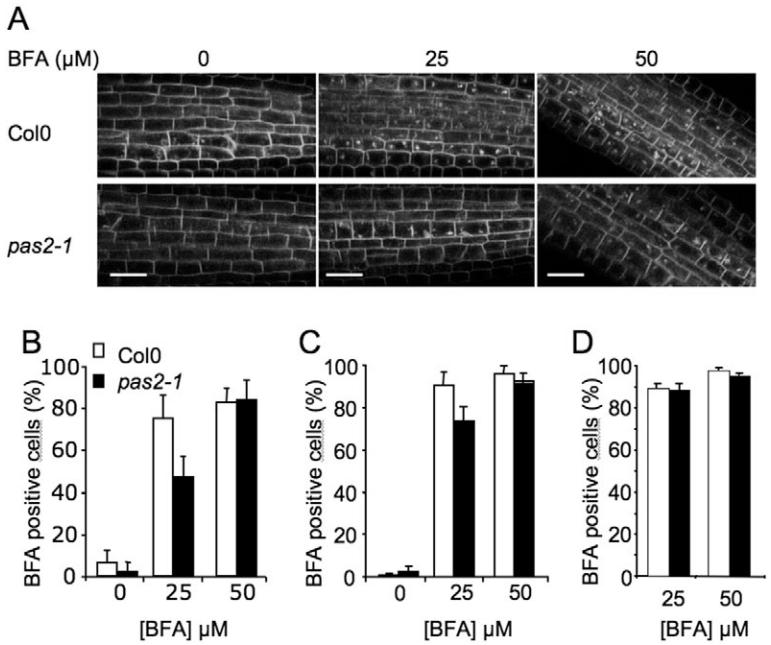


**Fig. 7. The pas2-1 mutant shows reduced sensivity to BFA.** (**A**) Treatment of wild-type (left) and *pas2-1* (right) roots expressing *pPIN1:PIN1-GFP* with different BFA concentrations. *pas2-1* mutation decreased significantly the number of BFA compartments compared with the wild type. Scale bars: 20 μm. (**B**–**D**) BFA sensitivity of *pas2-1* mutant. The presence of PIN1–GFP (B) and YFP–RabA2$^{a}$ (C) markers in BFA compartment was reduced in *pas2-1* compared with the wild type. By contrast, the presence of the Golgi maker QUA2–GFP in the BFA compartment was not modified (D). The relative number of cells in the stele showing GFP or YFP in BFA compartments was determined in wild-type and *pas2-1* primary root. Data are means + s.d. ($n$=30).

cuticular waxes and triacylgycerols, and also of sphingolipids and phospholipids (Bach et al., 2008). Interestingly, perturbations of the levels of VLCFAs in glycerolipids and sphingolipids led to curved thylakoid membranes and to defective endocytic membrane traffic, respectively (Millar et al., 1998; Zheng et al., 2005). The root-specific lipid suberin, a VLCFA-containing extracellular biopolymer restricted to perivascular cells (Franke and Schreiber, 2007), has also been shown to have a role in root development. Moreover, the double mutant *kcs20,daisy-1* and also the *kcr1* RNAi lines showed specific reduction of VLCFAs in suberin and they exhibited reduced root growth and an abnormal root phenotype associated with an inhibition of lateral root initiation and root hair elongation (Beaudoin et al., 2009; Lee et al., 2009). None of these phenotypes was observed in the *pas2-1* mutant, suggesting that cytokinesis defects observed in the root are not caused by defective suberin synthesis but most probably by the reduction of VLCFAs in phospholipids and sphingolipids. The involvement of VLCFAs in cytokinesis was confirmed by the occurrence of a defective cell plate, ectopic KNOLLE labeling and YFP–RabA2a aggregation in the other *pas* mutants, and also in cells treated with the specific elongase inhibitor flufenacet. Polar VLCFA-containing lipids are major constituents of plasma membrane (along with sterols). Previous studies of the cyclopropylsterol isomerase *cpi1-1* mutant demonstrated that sterol membrane composition was essential for differential endocytosis during cell plate maturation (Boutte et al., 2009; Men et al., 2008). The *pas2-1* mutation caused cytokinesis defects resembling those of *cpi1-1* mutant because it too exhibited unfused KNOLLE-positive cell-plate-like structures and KNOLLE mislocalization on the lateral membrane of dividing cells. However, sterol levels were not reduced in *pas2-1* cells, but instead were elevated, indicating that *pas2-1* cell plate defects were not caused by sterol depletion, and that VLCFA and sterols underpin similar cellular processes. Such a compensatory increase of sterol levels was also observed in the VLCFA-depleted *pas1* mutant and also in sphingolipid-deficient yeast mutants (Guan et al., 2009; Roudier et al., 2010).

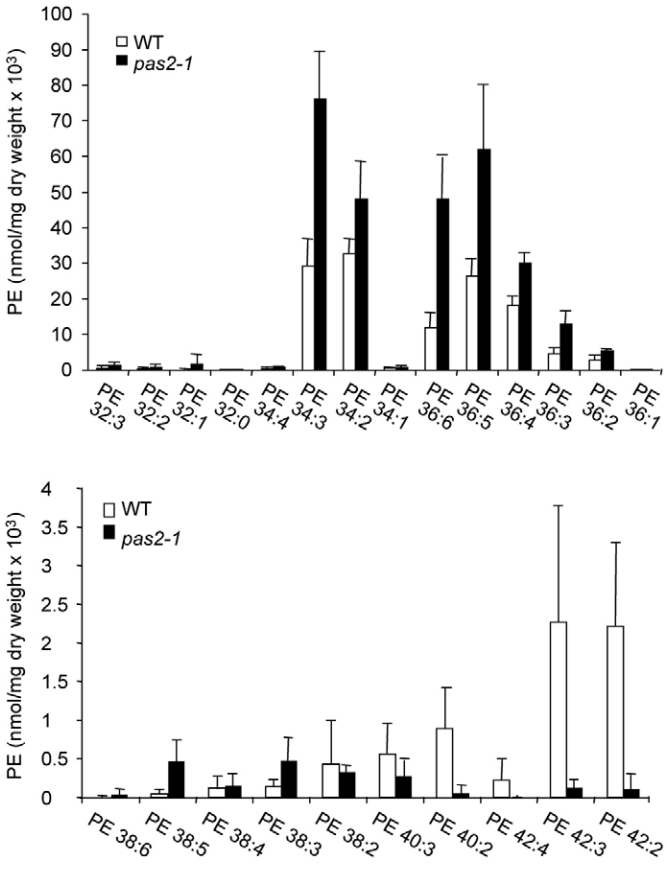


**Fig. 8. *pas2-1* mutant exhibits reduced levels of VCLFA-containing phosphatidylethanolamine.** Fatty acyl chain length composition of phosphatidylethanolamine fraction (PE) in 15-day-old WT and *pas2-1* mutant roots. PEs were separated according to their acyl chain length, long acyl chains (top) and very long acyl chains (bottom). Data are means + s.d.

Although it is clear that the secretory pathway is strongly involved in cell plate formation, the role of endocytosis remains a source of debate. Indeed, it has been reported that the styryl dye FM4-64 and fluid-phase markers such as Alexa Fluor 633 rapidly label the forming cell plate within minutes (Dhonukshe et al., 2006). The discovery of a BFA-resistant ARF-GEF GNOM-LIKE1 (GNL1) would explain the insensivity of the cell plate to BFA (Reichardt et al., 2007) because the *gnl1* mutant seedlings treated with BFA (mimicking the *gnl1,gn* double mutant), showed KNOLLE blocked in the ER and cytokinesis defects resembling those in *KNOLLE* mutants (Teh and Moore, 2007). FM4-64 pulse-chase experiments in the *pas2-1* mutant support the role of VLCFA during endocytosis at least in interphasic cells. Reduced endocytosis could also explain the relative insensitivity of PIN1–GFP and YFP–RabA2[a] to BFA in *pas2-1* cells. Endocytosis inhibition in *pas2-1* would indeed reduce PIN1 recycling throughout the endosomal compartments and therefore could at least partially explain its reduced accumulation upon BFA inhibition. Finally, the pattern of KNOLLE localization in *pas2-1* argues in favour of defective endocytosis during late cytokinesis. Indeed, KNOLLE is normally removed from the cell plate by endocytosis and targeted into multivesicular bodies or prevacuolar compartments in late mitotic cells (Dhonukshe et al., 2006; Reichardt et al., 2007; Teh and Moore, 2007). The finding that KNOLLE was retained in the ectopic cell plate in interphase cells and that it was mislocalized on lateral membrane in dividing cells are clear signatures of defective endocytosis (Boutte et al., 2009).

Most of the cytokinesis defects associated with PAS2-dependent VLCFA synthesis involved membrane dynamics associated with (most probably) endocytosis. However, the secretory pathway would be more important during cell plate expansion than initiation, as suggested by normal recovery of YFP–RabA2a after photobleaching in expanding *pas2-1* cell plate. The presence of two growth phases in *pas2-1* cell plate expansion could also be explained by the existence of two different processes: the first stages of cell plate emergence might require the provision of VLCFA-containing lipids provided by the secretory pathway, and later, the cell plate expansion would require mainly endocytosis of pre-existing plasma membrane material.

The most straightforward explanation would be that VLCFAs present in membrane lipids (phospholipids and sphingolipids) are necessary for vesicle transport, fusion and/or budding, as a consequence of their biophysical properties. In yeast, acyl chain length was found to be of crucial importance for such functions. In particular, C26-VLCFAs have been demonstrated to be necessary in protein trafficking and protein stability (Eisenkolb et al., 2002). A connection between VLCFA synthesis and membrane biophysical properties was provided by the observation that the conditional yeast acetyl-CoA carboxylase mutant *acc1*$^{ts}$*,mtr7* was affected in the structure and the function of the nuclear envelope (Al-Feel et al., 2003). Crucially, the C26 phosphatidylinositol (but not sphingolipids or GPI anchors with similar VLCFAs) was shown to be critical for membrane bending, probably by stabilizing the highly negative curvature of the membrane (Schneiter et al., 2004). Similar findings were observed in animals, where membrane curvature of the plasma membrane during furrow ingression is dependent on the VLCFA content (Szafer-Glusman et al., 2008).

Finally, our data demonstrated that VCLFAs are essential for plant cell division by controlling endomembrane dynamics. Although the exact roles of the different VLCFA-containing lipid classes in the formation of the new cell plate remain to be determined, the availability of mutants in the different biosynthetic pathways and the development of specific subcellular markers will provide the appropriate tools to further dissect the structural role of these lipids during cytokinesis in plants.

## Materials and Methods

### Plant materials

*Arabidopsis thaliana* Columbia-0 accession (Col0), *pas1-2*, *pas2-1* and *pas3-1* heterozygous mutants (EMS alleles in Col0 background) were used for this study. The *pas2-1* heterozygous line carrying the GUS fusion with cyclin B1 and its destruction box (db) *pCYCB1:db-GUS* (Doerner et al., 1996) was described previously (Harrar et al., 2003). The *pPIN1:PIN1-GFP*, *pRab-A2:YFP-RabA2* and *pSNX1:SNX1-GFP*, *p35S:GFP-RabF2b* constructs (Vernoux et al., 2000; Chow et al., 2008) were crossed into *pas2-1* mutant. *pPAS2:PAS2-GFP* construct (Bach et al., 2008) and were stably transferred into *pas2-1* heterozygous line by *Agrobacterium tumefaciens* flower dip transformation. Representative lines were selected from several independent transformants for further analyses. Plants were grown in greenhouse on soil (Tref Substrates, Rotterdam, The Netherlands) and watered with Plant-Prod nutritive solution (Fertil, Boulogne Billancourt, France). Seedlings were germinated on vertically oriented *Arabidopsis* agar medium (Estelle and Sommerville, 1987) and grown under constant temperature 18℃, 16 hour light, 8 hour dark cycle and with 60% hygrometry. Analyses were carried out on 5-day-old seedlings. Statistical analysis for supplementary material Fig. S1 and Figs 1 and 2 was carried out by applying Student's *t*-test with $P \leq 0.05$.

### Staining and inhibitors treatments

GUS staining was carried out as described previously (Harrar et al., 2003). Analysis of the cell plate formation was performed on seedlings incubated for 5 minutes in 8 μM FM4-64 (Invitrogen) and immediately mounted on slides. To observe FM4-64 internalization, 5-day-old seedlings were stained in 8 μM FM-64 for 3 minutes and washed in water before imaging. BFA (Sigma) was applied to seedlings to final concentrations of 25 μM and 50 μM for 30 minutes. Treated seedlings were mounted with FM4-64 and imaged for 30 minutes. Seeds of fluorescent marker lines were germinated on *Arabidopsis* medium supplemented with 75 nM Flufenacet (Sigma) and 7-day-old roots were imaged.

### Immunofluorescence localization

Whole-mount preparations were carried out according to published results (Friml et al., 2003) and modified according to Bolte and colleagues (Bolte et al., 2007). Seedlings were mounted on slides with one drop of anti-fading solution (Vectashield) with DAPI (100 μM; Roche) and coverslips were placed on top. Slides were stored 3 days at 4℃ and then visualized by confocal microscopy. The antibodies and dilutions used are listed below: rabbit anti-KNOLLE, 1:2000; mouse anti-α-tubulin (Invitrogen), 1:500. Alexa Fluor 488 goat anti-rabbit, Alexa Fluor 568 goat anti-mouse, Alexa Fluor 568 goat anti-rabbit, secondary antibodies were diluted at 1:500.

### Immunofluorescence microscopy

Root-tip cells were imaged with a Zeiss LSM710 confocal microscope using a 405 nm diode laser line exciting DAPI, a 488 nm argon laser line exciting Alexa Fluor 488 and a 561 nm diode laser line exciting Alexa Fluor 568. Fluorescence emission was detected between 410 and 480 nm for DAPI, 495–530 nm for Alexa Fluor 488 and 565–600 nm for Alexa Fluor 568. In multi-labelling studies, detection was performed in a sequential line-scanning mode with a line average of eight. Images were analysed using ZEN (Zeiss) and IMAGE J software.

### Live-cell imaging

Live-cell analysis of root-tip seedlings was performed on the Zeiss LSM710 confocal microscope. Fluorescence was recorded after a 488 nm (GFP) or 514 nm (YFP and FM4-64) excitation and a selective emission of 495–525 nm for GFP, 520–550 nm for YFP and 600–700 nm for FM4-64. Time-lapse analysis of YFP was carried out with low laser output and a large YFP emission bandwidth to minimize photobleaching. Some bleedthrough of FM4-64 staining could thus be observed in the YFP channel as shown by YFP-RabA2a plasma membrane labelling. Elongation zone length was defined as the distance from the last epidermal meristematic cell to the first differentiated cell with a root hair bulge. Division zone length was defined as the position from the quiescent centre to the position of the first rapidly elongating epidermal cell. Cell size of 5-day-old seedlings was measured with ImageJ, and the values were gathered and processed in Microsoft Excel.

### High-pressure freezing, freeze substitution and embedding processes

Root tips (3 mm) were cut in 1-hexadecen, transferred to a 200 µm size cupule (Leica, ref. 16706897) containing 1-hexadecen and frozen with a high-pressure freezer apparatus (EMPACT2, Leica, France). Freeze substitution was carried out (Leica freeze substitution unit AFS2, Leica, France) in acetone supplemented with 2% osmium tetroxide warming up progressively from –90℃ to –30℃ (specimens were left at –90℃ for 27 hours, then warmed up to –60℃ over 15 hours). Specimens were placed in a –60˚ bath for 8 hours, before the next warm-up step to –30℃ over 15 hours, where they remain for additional 8 hours. Root tips were finally infiltrated and embedded in epoxy resin (Low Viscosity Premix Kit-medium, Agar) at room temperature according to the manufacturer's instructions. For polymerization, they were placed in flat plastic moulds and polymerized for 17 hours at 60℃.

### Electron microscopy observations

70 nm ultrathin sections (Ultracut UC6, Leica) were collected on formvar-coated copper grids and poststained with aqueous 2% uranyl acetate and lead citrate as described (Hawes and Satiat-Jeunemaitre, 2001). They were examined with a JEOL 1400 transmission electron microscope (Croissy, France) operating at 120 kV. Images were acquired using a post-column high-resolution (11 megapixel) high-speed camera (SC1000 Orius, Gatan).

### Phospholipid analysis

Phospholipid analyses were performed at the Kansas Lipidomics Research Center, as described (Welti et al., 2002). For sterol analysis, total lipids were loaded onto HPTLC plates developed in hexane, ethylether and acetic acid (90:15:2; v/v/v) and separated into diacylglycerols ($R_F$ 0.08), sterols ($R_F$ 0.17), fatty alcohols ($R_F$ 0.22) and free fatty acids ($R_F$ 0.29).

## Acknowledgements

We thank Ian Moore, Thierry Gaude, Karin Schumacher and Gerd Jürgens for respectively for the gifts of pRab-A2:YFP-Rab-A2a, p35S:GFP-RabF2b and p35S:VHAa1-GFP transgenic lines and for KNOLLE antibodies. We thank Jan Traas and Jose Estevez for the gift of pPIN1-PIN1:GFP and LeAGP1-GFP transgenic lines respectively. We thank Bruno Letarnec for taking care of the plants. Rothamsted Research receives grant-aided support from the BBSRC (UK). This work has used the IJPB cytology and imaging facility and the plant chemistry facility (supported by Region Ile de France and Conseil Général des Yvelines) as well as the Electron Microscopy facilities and Cell biology unit of the Imagif platform (CNRS, supported by the Conseil General de l'Essonne, www.imagif.cnrs.fr). The author responsible for distribution of materials presented in this article is Jean-Denis Faure.

## Funding

L.B. was funded by Bourse Canceropôle Ile de France. This work was supported by the ANR programe blanc SphingopolaR (07-BLAN-202).

## References

**Al-Feel, W., DeMar, J. C. and Wakil, S. J.** (2003). A *Saccharomyces cerevisiae* mutant strain defective in acetyl-CoA carboxylase arrests at the G2/M phase of the cell cycle. *Proc. Natl. Acad. Sci. USA* **100**, 3095-3100.

**Alberts, B., Johnson, A., Lewis, J., Raff, M., Roberts, K. and Walter, P.** (2002). *Molecular Biology of the Cell*, (4th edn). New York: Garland Science.

**Bach, L. and Faure, J. D.** (2010). Role of very-long-chain fatty acids in plant development, when chain length does matter. *C. R. Biol.* **333**, 361-370.

**Bach, L., Michaelson, L., Haslam, R., Bellec, Y., Gissot, L., Marion, J., Da Costa, M., Boutin, J.-P., Miquel, M., Tellier, F. et al.** (2008). The plant very long chain hydroxy fatty Acyl-CoA dehydratase PASTICCINO2 is essential and limiting for plant development. *Proc. Natl. Acad. Sci. USA* **105**, 14727-14731.

**Beaudoin, F., Wu, X., Li, F., Haslam, R. P., Markham, J. E., Zheng, H., Napier, J. A. and Kunst, L.** (2009). Functional characterization of the *Arabidopsis* beta-ketoacyl-coenzyme A reductase candidates of the fatty acid elongase. *Plant Physiol.* **150**, 1174-1191.

**Bellec, Y., Harrar, Y., Butaeye, C., Darnet, S., Bellini, C. and Faure, J. D.** (2002). Pasticcino2 is a protein tyrosine phosphatase-like involved in cell proliferation and differentiation in *Arabidopsis*. *Plant J.* **32**, 713-722.

**Bolte, S., Boutt, Y., Kluge, C., Brown, S. and Satiat-Jeunemaitre, B.** (2007). Tracking gene expression in plant cells: new probes for functional genomics. In *Functional Plant Genomics* (J.-F. Morot-Gaudry, P. Lea and J.F. Briat eds), pp. 277-310. Boca Raton, FL: CRC Press.

**Borner, G. H., Sherrier, D. J., Weimar, T., Michaelson, L. V., Hawkins, N. D., Macaskill, A., Napier, J. A., Beale, M. H., Lilley, K. S. and Dupree, P.** (2005). Analysis of detergent-resistant membranes in *Arabidopsis*. Evidence for plasma membrane lipid rafts. *Plant Physiol.* **137**, 104-116.

**Boutte, Y., Crosnier, M. T., Carraro, N., Traas, J. and Satiat-Jeunemaitre, B.** (2006). The plasma membrane recycling pathway and cell polarity in plants: studies on PIN proteins. *J. Cell Sci.* **119**, 1255-1265.

**Boutte, Y., Frescatada-Rosa, M., Men, S., Chow, C. M., Ebine, K., Gustavsson, A., Johansson, L., Ueda, T., Moore, I., Jurgens, G. et al.** (2009). Endocytosis restricts *Arabidopsis* KNOLLE syntaxin to the cell division plane during late cytokinesis. *EMBO J.* **29**, 546-558.

**Chen, X. Y., Liu, L., Lee, E., Han, X., Rim, Y., Chu, H., Kim, S. W., Sack, F. and Kim, J. Y.** (2009). The *Arabidopsis* callose synthase gene GSL8 is required for cytokinesis and cell patterning. *Plant Physiol.* **150**, 105-113.

**Chow, C. M., Neto, H., Foucart, C. and Moore, I.** (2008). Rab-A2 and Rab-A3 GTPases define a trans-golgi endosomal membrane domain in *Arabidopsis* that contributes substantially to the cell plate. *Plant Cell* **20**, 101-123.

**Dettmer, J., Hong-Hermesdorf, A., Stierhof, Y. D. and Schumacher, K.** (2006). Vacuolar H+-ATPase activity is required for endocytic and secretory trafficking in *Arabidopsis*. *Plant Cell* **18**, 715-730.

**Dhonukshe, P., Baluska, F., Schlicht, M., Hlavacka, A., Samaj, J., Friml, J. and Gadella, T. W., Jr** (2006). Endocytosis of cell surface material mediates cell plate formation during plant cytokinesis. *Dev. Cell* **10**, 137-150.

**Doerner, P., Jorgensen, J. E., You, R., Steppuhn, J. and Lamb, C.** (1996). Control of root growth and development by cyclin expression. *Nature* **380**, 520-523.

**Dunn, T. M., Lynch, D. V., Michaelson, L. V. and Napier, J. A.** (2004). A post-genomic approach to understanding sphingolipid metabolism in *Arabidopsis thaliana*. *Ann. Bot.* **93**, 483-497.

**Eisenkolb, M., Zenzmaier, C., Leitner, E. and Schneiter, R.** (2002). A specific structural requirement for ergosterol in long-chain fatty acid synthesis mutants important for maintaining raft domains in yeast. *Mol. Biol. Cell* **13**, 4414-4428.

**Estevez, J. M., Kieliszewski, M. J., Khitrov, N. and Somerville, C.** (2006). Characterization of synthetic hydroxyproline-rich proteoglycans with arabinogalactan protein and extensin motifs in Arabidopsis. *Plant Physiol.* **142**, 458-470.

**Faure, J. D., Vittorioso, P., Santoni, V., Fraisier, V., Prinsen, E., Barlier, I., Vanonckelen, H., Caboche, M. and Bellini, C.** (1998). The PASTICCINO genes of *Arabidopsis thaliana* are involved in the control of cell division and differentiation. *Development* **125**, 909-918.

**Franke, R. and Schreiber, L.** (2007). Suberin-a biopolyester forming apoplastic plant interfaces. *Curr. Opin. Plant Biol.* **10**, 252-259.

**Friml, J., Benkova, E., Mayer, U., Palme, K. and Muster, G.** (2003). Automated whole mount localisation techniques for plant seedlings. *Plant J.* **34**, 115-124.

**Geldner, N., Anders, N., Wolters, H., Keicher, J., Kornberger, W., Muller, P., Delbarre, A., Ueda, T., Nakano, A. and Jurgens, G.** (2003). The *Arabidopsis* GNOM ARF-GEF mediates endosomal recycling, auxin transport, and auxin-dependent plant growth. *Cell* **112**, 219-230.

**Guan, X. L., Souza, C. M., Pichler, H., Dewhurst, G., Schaad, O., Kajiwara, K., Wakabayashi, H., Ivanova, T., Castillon, G. A., Piccolis, M. et al.** (2009). Functional interactions between sphingolipids and sterols in biological membranes regulating cell physiology. *Mol. Biol. Cell* **20**, 2083-2095.

**Harrar, Y., Bellec, Y., Bellini, C. and Faure, J. D.** (2003). Hormonal control of cell proliferation requires PASTICCINO genes. *Plant Physiol.* **132**, 1217-1227.

**Hawes, C. R. and Satiat-Jeunemaitre, B.** (2001). Trekking along the cytoskeleton. *Plant Physiol.* **125**, 119-122.

**Hepler, P. K. and Bonsignore C. L.** (1990). Caffein inhibition of cytokinesis: ultrastructure of cell plate formation/degradation. *Protoplasma* **157**, 182-192.

**Ikonen, E.** (2001). Roles of lipid rafts in membrane transport. *Curr. Opin. Cell Biol.* **13**, 470-477.

**Jürgens, G. and Pacher, T.** (2004). Cytokinesis: membrane trafficking by default? In *The Golgi Appartus and the Plant Secretory Pathways* (ed. D. G. Robinson), pp. 238-254. Oxford: Blackwell.

**Lauber, M. H., Waizenegger, I., Steinmann, T., Schwarz, H., Mayer, U., Hwang, I., Lukowitz, W. and Jurgens, G.** (1997). The *Arabidopsis* KNOLLE protein is a cytokinesis-specific syntaxin. *J. Cell Biol.* **139**, 1485-1493.

**Lee, S. B., Jung, S. J., Go, Y. S., Kim, H. U., Kim, J. K., Cho, H. J., Park, O. K. and Suh, M. C.** (2009). Two *Arabidopsis* 3-ketoacyl CoA synthase genes, KCS20 and KCS2/DAISY, are functionally redundant in cuticular wax and root suberin biosynthesis, but differentially controlled by osmotic stress. *Plant J.* **60**, 462-475.

**Lingwood, D. and Simons, K.** (2010). Lipid rafts as a membrane-organizing principle. *Science* **327**, 46-50.

**Lipka, V., Kwon, C. and Panstruga, R.** (2007). SNARE-ware: the role of SNARE-domain proteins in plant biology. *Annu. Rev. Cell Dev. Biol.* **23**, 147-174.

**Men, S., Boutte, Y., Ikeda, Y., Li, X., Palme, K., Stierhof, Y. D., Hartmann, M. A., Moritz, T. and Grebe, M.** (2008). Sterol-dependent endocytosis mediates post-cytokinetic acquisition of PIN2 auxin efflux carrier polarity. *Nat. Cell Biol.* **10**, 237-244.

**Millar, A. A., Wrischer, M. and Kunst, L.** (1998). Accumulation of very-long-chain fatty acids in membrane glycerolipids is associated with dramatic alterations in plant morphology. *Plant Cell* **10**, 1889-1902.

**Mima, J. and Wickner, W.** (2009). Complex lipid requirements for SNARE- and SNARE chaperone-dependent membrane fusion. *J. Biol. Chem.* **284**, 27114-27122.

**Molendijk, A. J., Ruperti, B. and Palme, K.** (2004). Small GTPases in vesicle trafficking. *Curr. Opin. Plant Biol.* **7**, 694-700.

**Mongrand, S., Morel, J., Laroche, J., Claverol, S., Carde, J. P., Hartmann, M. A., Bonneu, M., Simon-Plas, F., Lessire, R. and Bessoule, J. J.** (2004). Lipid rafts in higher plant cells: purification and characterization of Triton X-100-insoluble microdomains from tobacco plasma membrane. *J. Biol. Chem.* **279**, 36277-36286.

**Moreau, P., Juguelin, H., Cassagne, C. and Morre, D. J.** (1992). Molecular basis for low temperature compartment formation by transitional endoplasmic reticulum of rat liver. *FEBS Lett.* **310**, 223-228.

**Mouille, G., Ralet, M. C., Cavelier, C., Eland, C., Effroy, D., Hematy, K., McCartney, L., Truong, H. N., Gaudon, V., Thibault, J. F. et al.** (2007). Homogalacturonan synthesis in *Arabidopsis thaliana* requires a Golgi-localized protein with a putative methyltransferase domain. *Plant J.* **50**, 605-614.

**Nugteren, D. H.** (1965). The enzymic chain elongation of fatty acids by rat-liver microsomes. *Biochim. Biophys. Acta* **106**, 280-290.

**Paul, S., Gable, K., Beaudoin, F., Cahoon, E., Jaworski, J., Napier, J. A. and Dunn, T. M.** (2006). Members of the *Arabidopsis* FAE1-like 3-ketoacyl-CoA synthase gene family substitute for the Elop proteins of Saccharomyces cerevisiae. *J. Biol. Chem.* **281**, 9018-9029.

**Reichardt, I., Stierhof, Y. D., Mayer, U., Richter, S., Schwarz, H., Schumacher, K. and Jurgens, G.** (2007). Plant cytokinesis requires de novo secretory trafficking but not endocytosis. *Curr. Biol.* **17**, 2047-2053.

**Renault, L., Christova, P., Guibert, B., Pasqualato, S. and Cherfils, J.** (2002). Mechanism of domain closure of Sec7 domains and role in BFA sensitivity. *Biochemistry* **41**, 3605-3612.

**Roudier, F., Gissot, L., Beaudoin, F., Haslam, R., Michaelson, L., Marion, J., Molino, D., Lima, A., Bach, L., Morin, H. et al.** (2010). Very-long-chain fatty acids are involved in polar auxin transport and developmental patterning in *Arabidopsis*. *Plant Cell* **22**, 364-375.

**Samuels, A. L., Giddings, T. H., Jr and Staehelin, L. A.** (1995). Cytokinesis in tobacco BY-2 and root tip cells: a new model of cell plate formation in higher plants. *J. Cell Biol.* **130**, 1345-1357.

**Schneiter, R., Hitomi, M., Ivessa, A. S., Fasch, E. V., Kohlwein, S. D. and Tartakoff, A. M.** (1996). A yeast acetyl coenzyme A carboxylase mutant links very-long-chain fatty acid synthesis to the structure and function of the nuclear membrane-pore complex. *Mol. Cell. Biol.* **16**, 7161-7172.

**Schneiter, R., Brugger, B., Amann, C. M., Prestwich, G. D., Epand, R. F., Zellnig, G., Wieland, F. T. and Epand, R. M.** (2004). Identification and biophysical characterization of a very-long-chain-fatty-acid-substituted phosphatidylinositol in yeast subcellular membranes. *Biochem. J.* **381**, 941-949.

**Segui-Simarro, J. M., Austin, J. R., 2nd, White, E. A. and Staehelin, L. A.** (2004). Electron tomographic analysis of somatic cell plate formation in meristematic cells of *Arabidopsis* preserved by high-pressure freezing. *Plant Cell* **16**, 836-856.

**Steinmann, T., Geldner, N., Grebe, M., Mangold, S., Jackson, C. L., Paris, S., Galweiler, L., Palme, K. and Jurgens, G.** (1999). Coordinated polar localization of auxin efflux carrier PIN1 by GNOM ARF GEF. *Science* **286**, 316-318.

**Szafer-Glusman, E., Giansanti, M. G., Nishihama, R., Bolival, B., Pringle, J., Gatti, M. and Fuller, M. T.** (2008). A role for very-long-chain fatty acids in furrow ingression during cytokinesis in *Drosophila* spermatocytes. *Curr. Biol.* **18**, 1426-1431.

**Teh, O. K. and Moore, I.** (2007). An ARF-GEF acting at the Golgi and in selective endocytosis in polarized plant cells. *Nature* **448**, 493-496.

**Trenkamp, S., Martin, W. and Tietjen, K.** (2004). Specific and differential inhibition of very-long-chain fatty acid elongases from *Arabidopsis thaliana* by different herbicides. *Proc. Natl. Acad. Sci. USA* **101**, 11903-11908.

**Van Damme, D., Inze, D. and Russinova, E.** (2008). Vesicle trafficking during somatic cytokinesis. *Plant Physiol.* **147**, 1544-1552.

**van Meer, G.** (1989). Lipid traffic in animal cells. *Annu. Rev. Cell Biol.* **5**, 247-275.

**Vernoux, T., Kronenberger, J., Grandjean, O., Laufs, P. and Traas, J.** (2000). PIN-FORMED 1 regulates cell fate at the periphery of the shoot apical meristem. *Development* **127**, 5157-5165.

**Wang, Q. and Chang, A.** (2002). Sphingoid base synthesis is required for oligomerization and cell surface stability of the yeast plasma membrane ATPase, Pma1. *Proc. Natl. Acad. Sci. USA* **99**, 12853-12858.

**Welti, R., Li, W., Li, M., Sang, Y., Biesiada, H., Zhou, H. E., Rajashekar, C. B., Williams, T. D. and Wang, X.** (2002). Profiling membrane lipids in plant stress responses. Role of phospholipase D alpha in freezing-induced lipid changes in *Arabidopsis*. *J. Biol. Chem.* **277**, 31994-2002.

**Westerberg, R., Tvrdik, P., Unden, A. B., Mansson, J. E., Norlen, L., Jakobsson, A., Holleran, W. H., Elias, P. M., Asadi, A., Flodby, P. et al.** (2004). Role for ELOVL3 and fatty acid chain length in development of hair and skin function. *J. Biol. Chem.* **279**, 5621-5629.

**Zheng, H., Rowland, O. and Kunst, L.** (2005). Disruptions of the *Arabidopsis* Enoyl-CoA reductase gene reveal an essential role for very-long-chain fatty acid synthesis in cell expansion during plant morphogenesis. *Plant Cell* **17**, 1467-1481.